Atmos. Chem. Phys. Discuss., 15, 11573–11597, 2015
www.atmos-chem-phys-discuss.net/15/11573/2015/
doi:10.5194/acpd-15-11573-2015

Atmospheric Chemistry and Physics Discussions

Impact of ozone observations on the structure of a tropical cyclone using coupled atmosphere–chemistry data assimilation

S. Lim[1,3,4], **S. K. Park**[1,2,3,4], **and M. Zupanski**[5]

[1]Department of Atmospheric Science and Engineering, Ewha Womans University, Seoul, Republic of Korea
[2]Department of Environmental Science and Engineering, Ewha Womans University, Seoul, Republic of Korea
[3]Center for Climate/Environment Change Prediction Research, Ewha Womans University, Seoul, Republic of Korea
[4]Severe Storm Research Center, Ewha Womans University, Seoul, Republic of Korea
[5]Cooperative Institute for Research in the Atmosphere, Colorado State University, Fort Collins, CO, USA

Received: 30 January 2015 – Accepted: 23 March 2015 – Published: 21 April 2015

Correspondence to: S. K. Park (spark@ewha.ac.kr)

Published by Copernicus Publications on behalf of the European Geosciences Union.

ACPD
15, 11573–11597, 2015

Abstract

Since the air quality forecast is related to both chemistry and meteorology, the coupled atmosphere–chemistry data assimilation (DA) system is essential to air quality forecasting. Ozone (O_3) plays an important role in chemical reactions and is usually assimilated in chemical DA. In tropical cyclones (TCs), O_3 usually shows a lower concentration inside the eyewall and an elevated concentration around the eye, impacting atmospheric as well as chemical variables. To identify the impact of O_3 observations on TC structure, including atmospheric and chemical information, we employed the Weather Research and Forecasting model coupled with Chemistry (WRF-Chem) with an ensemble-based DA algorithm – the maximum likelihood ensemble filter (MLEF). For a TC case that occurred over the East Asia, our results indicate that the ensemble forecast is reasonable, accompanied with larger background state uncertainty over the TC, and also over eastern China. Similarly, the assimilation of O_3 observations impacts atmospheric and chemical variables near the TC and over eastern China. The strongest impact on air quality in the lower troposphere was over China, likely due to the pollution advection. In the vicinity of the TC, however, the strongest impact on chemical variables adjustment was at higher levels. The impact on atmospheric variables was similar in both over China and near the TC. The analysis results are validated using several measures that include the cost function, root-mean-squared error with respect to observations, and degrees of freedom for signal (DFS). All measures indicate a positive impact of DA on the analysis – the cost function and root mean square error have decreased by 16.9 and 8.87 %, respectively. In particular, the DFS indicates a strong positive impact of observations in the TC area, with a weaker maximum over northeast China.

ACPD
15, 11573–11597, 2015

1 Introduction

The air quality forecast is related to emissions, transport, transformation and removal processes, and to the prevailing meteorological conditions. Therefore, the coupled atmosphere–chemistry model is essential for the air quality and weather forecasting (e.g., Carmichael et al., 2008). The coupled system forecast is improved through coupled atmosphere–chemistry data assimilation (DA), which estimates the best initial conditions by blending the model and observations (e.g., Houtekamer and Mitchell, 1998; Elbern and Schmidt, 1999; Wang et al., 2001; Evensen, 2003; Park and Zupanski, 2003; Navon, 2009; Zupanski, 2009).

Ozone (O_3) is usually assimilated in a chemical DA because it represents the atmospheric flow as a passive tracer at synoptic or smaller scales and has a relatively long photochemical lifetime and high concentrations in the stratosphere, except during ozone hole conditions, and at high latitudes (e.g., Lahoz et al., 2007; Wu and Zou, 2008). Moreover, the improved stratospheric O_3 distribution by DA can affect atmospheric variables such as stratospheric winds and temperature as well as other chemical variables (e.g., Lahoz et al., 2007).

O_3 is also relevant to the structure of tropical cyclones (TCs), showing a lower concentration just inside the eyewall and elevated concentration around the eye (e.g., Carsey and Willoughby, 2005; Zou and Wu, 2005; Wu and Zou, 2008), which is caused by the updraft in the eyewall and subsidence in the eye (Zou and Wu, 2005). Using these relations, the daily total column O_3 from Total Ozone Mapping Spectrometer (TOMS) showed that mutual adjustment occurred between the TC and its upper tropospheric environment on a synoptical timescale (Rodgers et al., 1990; Stout and Rodgers, 1992). The linear relationship between total column O_3 from TOMS and mean vertically-integrated potential vorticity (MPV) was used to improve hurricane or winter storm prediction (e.g., Jang et al., 2003; Wu and Zou, 2008; Zou and Wu, 2005). However, these studies employed an atmospheric model, not the coupled atmosphere–chemistry model. They used the standard dynamical variables as control variables and

ACPD
15, 11573–11597, 2015

empirical regressions to develop a cross-correlation between O_3 and dynamical model variables.

In this study, we directly assimilate the total column O_3 from the Ozone Monitoring Instrument (OMI) to identify the impact of O_3 observations on TC structure including atmospheric and chemical information in a coupled atmosphere–chemistry model (e.g., WRF-Chem) with ensemble-based DA system (e.g., Maximum Likelihood Ensemble Filter; MLEF). We define an augmented control variable that includes both dynamical and chemical variables. Therefore, the cross-correlations between dynamical and chemical variables are obtained directly from ensemble forecasts. Section 2 describes the methodology, and Sect. 3 presents results. Conclusions are provided in Sect. 4.

2 Methodology

2.1 Model

In this research, we use the Weather Research and Forecasting (WRF) model coupled with Chemistry (WRF-Chem) version 3.4.1 as a prediction model on a regional scale. It simulates the emission, transport, mixing and chemical transformation of trace gases and aerosols simultaneously with meteorology (Grell et al., 2005). The WRF-Chem uses configuration options for various atmospheric processes such as the WRF Single-Moment 6-class (WSM6) scheme for the microphysics, the Community Atmospheric Model (CAM) scheme for the radiation physics, the Monin–Obukhov scheme for the surface layer, the Noah land surface model for the land surface, the Yonsei University (YSU) scheme for the planetary boundary layer, and the Kain–Fritsch scheme for the cumulus parameterization. These are the recommended physics options for the regional climate case at 10–30 km grid size. As an advection option, the monotonic transport is applied to turbulent kinetic energy and scalars such as mixing ratios of water vapor, cloud water, rain, snow and ice and chemical species, which is commonly used for real-time and research applications (e.g., Chapman et al., 2009; Yang et al.,

ACPD
15, 11573–11597, 2015

2011). Regarding the chemical mechanism, the Carbon Bond Mechanism version Z (CBMZ) without Dimethylsulfide scheme is used for gas-phase chemistry.

In terms of the DA system, we use an ensemble-based DA method called the Maximum Likelihood Ensemble Filter (MLEF; Zupanski, 2005; Zupanski et al., 2008). The MLEF generates the analysis solution which maximizes the likelihood of the posterior probability distribution, obtained by minimization of a cost function. The MLEF belongs to the family of deterministic ensemble filters, hence it is a hybrid between variational and ensemble DA methods. The MLEF employs a cost function derived using a Gaussian probability density function and produces both the analysis and the background error covariance (Zupanski, 2005). It is well suited for use with highly nonlinear observation operators, for a small additional computational cost of minimization using the Hessian preconditioning (Zupanski, 2005; Zupanski et al., 2007, 2008).

2.2 Observations

Satellite retrievals often provide estimates of chemical concentration as a total vertical column, and they cover a wide geographical range compared to other measurements (e.g., Silver et al., 2013). In our study, the total column O_3 obtained by OMI is used as an observation. OMI is a nadir-viewing near-UV/Visible CCD spectrometer aboard NASA's Aura satellite (OMI Team, 2012). The total column O_3 is Level 2 data (OMTO3) based on the Total Ozone Mapping Spectrometer (TOMS) v8.5 algorithm, which is obtained from an orbital swath with a resolution of 13 km × 24 km at nadir (OMI Team, 2012). It achieves global coverage in one day. In this experiment, we did not apply the quality flags because the first appearance of the row anomaly that affects particular viewing directions, corresponding to the rows on the CCD detectors (OMI Team, 2012) did not occur in 2005, when the TC case considered occurred (i.e., Typhoon Nabi, 2005). Therefore, we employ the OMI data without quality flags.

Figure 1 shows the total column O_3 from OMI at 04:05 UTC 3 September 2005. It shows a lower concentration just inside the eyewall and elevated concentration around the eye. This distinct distribution is well described when the TC has the strongest in-

ACPD
15, 11573–11597, 2015

tensity in the intensifying stages (e.g., Carsey and Willoughby, 2005). Note that OMI switches from its normal global mode to zoom-in mode, to perform spatial zoom (higher resolution) measurements, for a 24 h period about once a month. It occurs when OMI finishes its last orbital pass over Europe, and returns to global mode after 14–15 orbits or about 24 h later. During this period of zoom-in mode, OMI has no global coverage of data (OMI Team, 2012). Typhoon Nabi (2005) reached the maximum intensity on 2 September when OMI entered in the zoom-in mode. Due to the lack of ozone data in our domain on 2 September, we have alternatively chosen 3 September for the analysis of O_3 properties during the maximum development of the TC case.

2.3 Experimental design

For the TC case, we choose Typhoon Nabi (2005), which lasted several days from 29 August 2005 until 8 September 2005. Nabi moved westward after its formation and passed near Saipan on 31 August as an intensifying TC, transformed to a super typhoon on 1 September, and reached its peak with winds of 175 $km\,h^{-1}$ (10-min average) on 2 September. It became weak while turning to the north and striking Kyushu on 6 September. Nabi turned to the northeast after passing by South Korea, and transformed to an extratropical cyclone passing over Hokkaido on 8 September.

We focused on a single DA cycle from 00:00 to 06:00 UTC 3 September 2005, which is one of the strongest periods of its lifetime. We conduct the experiment with 32 ensembles and 6 h assimilation window. Note that the OMI observations have an approximate frequency of once per day over the typhoon and the surrounding geographical area. Therefore, adding more data assimilation cycles would not be beneficial since no additional data are available. In the future we plan to add a capability to assimilate other observations, such as atmospheric observations and all-sky infrared radiances from a geostationary satellite.

The initial and lateral boundary conditions for atmospheric states are provided by the National Centers for Environmental Prediction (NCEP) Global Forecasting System (GFS), while those for chemical variables are obtained from the Model for Ozone and

ACPD
15, 11573–11597, 2015

Related chemical Tracers (MOZART) chemistry global model of the National Center for Atmospheric Research (NCAR)/Atmospheric Chemistry Division (ACD). The WRF-Chem is set up with a horizontal resolution of 30 km and 51 vertical levels with the bottom at the ground and the top at 10 hPa using a terrain-following hydrostatic pressure coordinate (Skamarock et al., 2008).

The model domain is centered over the Korean Peninsula, covering an area of approximately 3900 km × 4400 km with 132 × 147 horizontal grid points. The control variables defined in the coupled atmosphere–chemistry DA are the WRF-Chem prognostic variables that contain dynamical variables such as winds, perturbation potential temperature, perturbation geopotential, water vapor mixing ratio and perturbation dry air mass in a column, and the chemical variables such as ozone (O_3), nitrates (NO, NO_2, NO_3), and sulfur dioxide (SO_2). The experiments consist of (i) the forecast (without DA) which is useful to understand the synoptic situation and background error covariance, and (ii) the analysis (with DA) which is useful to understand the assimilation impacts.

2.4 Bias correction of total column O_3

We define the observation operator transforming the WRF-Chem O_3 forecast to the total column O_3 observation. It contains the calculation of total column O_3, unit conversion from ppmv (parts per million by volume) to Dobson Units (DU) and the bi-linear interpolation to the observation location. The most demanding part of the observation operator is bias correction of total column O_3 observation. Although we use the reference pressure at the model top as 10 hPa, which is the highest value we could use in the current model version, there are still considerable amounts of O_3 in the stratosphere that could not be included in the calculation of the model guess (e.g., background). Since this creates a negative bias in the mean observation error, we introduce a multiplicative bias correction ε to preserve positive-definiteness of the bias-corrected guess (Apodaca et al., 2014) as

$$h_B(\boldsymbol{x}) = \varepsilon \cdot h(\boldsymbol{x}). \quad (1)$$

ACPD
15, 11573–11597, 2015

With the multiplicative bias correction in Eq. (1), we can make a new cost function in unbiased form as

$$J(\boldsymbol{x}) = \frac{1}{2}(\boldsymbol{x} - \boldsymbol{x}_\mathrm{b})^\mathrm{T}\mathbf{P}_\mathrm{f}^{-1}(\boldsymbol{x} - \boldsymbol{x}_\mathrm{b}) + \frac{1}{2}[\boldsymbol{y} - h_B(\boldsymbol{x})]^\mathrm{T}\mathbf{R}^{-1}[\boldsymbol{y} - h_B(\boldsymbol{x})] \quad (2)$$

where $\boldsymbol{x}$ is the model state vector, $\boldsymbol{x}_\mathrm{b}$ is the prior (background) state, $\boldsymbol{y}$ is the observation vector, and the superscript T means a transpose. Here, h is the nonlinear observation operator, $\mathbf{P}_\mathrm{f}$ is the background (forecast) error covariance matrix in the ensemble subspace, and $\mathbf{R}$ is the observation error covariance matrix. Equation (2) is the cost function used in DA, provided ε can be estimated. The optimal value of parameter ε is obtained by implicitly assuming lognormal probability density function errors for a multiplicative bias correction in Eq. (1) (e.g., Apodaca et al., 2014) as

$$\varepsilon = \varepsilon_0 \exp\left[\frac{\frac{1}{N}\sum_{i=1}^{N}\log\left(\frac{\boldsymbol{y}_i}{\varepsilon_0 h(\boldsymbol{x})_i}\right)}{1 + \frac{r_0}{w_0}}\right] \quad (3)$$

where ε_0 is a guess parameter value and N is the number of observations. The empirical weighting values are set to $r_0 = w_0 = 0.5$ which implies having the same confidence in observations and the guess. We assume the starting value of the bias to be

$$\varepsilon_0 = \frac{\overline{\boldsymbol{y}}}{\overline{h(\boldsymbol{x})}} \quad \text{where} \quad \overline{\boldsymbol{y}} = \frac{1}{N}\sum_{i=1}^{N}\boldsymbol{y}_i, \quad \overline{h(\boldsymbol{x})} = \frac{1}{N}\sum_{i=1}^{N}h(\boldsymbol{x})_i \quad (4)$$

Equation (3) is calculated once in every DA cycle.

3 Results

A specific characteristic of our experiments is that both atmospheric and chemical variables are used as control variables in DA. Regarding the atmospheric variables, we

ACPD
15, 11573–11597, 2015

focus on what is related to the TC formation and development, such as the temperature, wind, and water vapor. Regarding the chemical variables, we select the chemical constituents such as O_3, NO_2 and SO_2. These are used to identify the impact of O_3 observations on the TC structure in a WRF-Chem-MLEF system.

3.1 Synoptic situation with ensemble WRF-Chem forecast

In general, observations show that SO_2 has larger concentrations in the troposphere while O_3 and NO_2 have larger concentrations in the stratosphere (e.g., Meena et al., 2006). However, in East Asia, especially in eastern China, there is a significant tropospheric NO_2 concentration because of the industrialized and urbanized part of China (Richter et al., 2005; Ohara et al., 2007). Regarding the atmospheric variables, temperature and water vapor have higher values in the troposphere, while wind has larger speed near the tropopause. To consider these characteristics, we focused on two pressure levels: (i) 850 hPa (lower troposphere) and (ii) 200 hPa (lower stratosphere). Our ensemble WRF-Chem forecast also supports these general distributions of control variables, which are not shown in this paper.

3.2 Background error covariance

The background error covariance represents the background state uncertainty (e.g., Kim et al., 2010). These are estimated by the difference between each of the 32 ensemble members and the control forecast in the ensemble system (Zhang et al., 2013). In our study, the ensemble WRF-Chem-MLEF estimates the background error covariance defined in Zupanski (2005) as

$$\mathbf{P}_\mathrm{f} = \mathbf{P}_\mathrm{f}^{1/2}\left(\mathbf{P}_\mathrm{f}^{1/2}\right)^\mathrm{T}, \quad \mathbf{P}_\mathrm{f}^{1/2} = \left(p_1^\mathrm{f}\cdots p_N^\mathrm{f}\right), \quad p_n^\mathrm{f} = m(\boldsymbol{x}_0^n) - m(\boldsymbol{x}_0) \tag{5}$$

where the index n is an ensemble member, N is the total number of ensemble forecasts, m is the WRF-Chem model, and the subscript 0 denotes the initial time of the

ACPD
15, 11573–11597, 2015

forecast with corresponding initial conditions $\boldsymbol{x}_0$ and ensemble initial conditions $\boldsymbol{x}_0^n$. In this experiment, the initial ensemble perturbations are generated by using the lagged forecast outputs (Zhang et al., 2013).

Being calculated from the WRF-Chem ensemble forecast, the flow-dependent background error covariance is defined for atmospheric and chemical variables, which allows chemistry observations to impact atmospheric variables in DA. In Zhang et al. (2013), a larger background state uncertainty was found in the storm region. Our results also identify the larger background state uncertainty near the TC, similar to Kim et al. (2010). Figure 2 shows the standard deviation (SD) of background error covariance for chemical variables. O_3 in particular (Fig. 2a and d, respectively) shows a large background state uncertainty near the TC, with the maximum of 0.024 ppmv at 200 hPa (Fig. 2d). The background state uncertainties of NO_2 and SO_2 at 200 hPa (Fig. 2e and f, respectively) are located near the TC, characterized by small magnitude and weak influence on tropospheric pollution. On the other hand, the background state uncertainties of NO_2 and SO_2 at 850 hPa (Fig. 2b and c, respectively) have more impact on central eastern China, implying no visible (or obvious) impact of the low-level NO_2 and SO_2 on the TC.

The SD of background error covariance for atmospheric variables appear to be more related to the TC structure (see Fig. 3). In particular, wind (Fig. 3a and d, respectively) shows a larger background state uncertainty near the TC at both pressure level, especially in the eye region at 850 hPa (Fig. 3a). Temperature (Fig. 3b and e, respectively) also shows a larger background state uncertainty near the TC, especially at 200 hPa (Fig. 3d). Regarding the water vapor mixing ratio (Fig. 3c and f, respectively), there is a larger background state uncertainty in the eye region at both pressure levels. Larger background state uncertainty potentially implies a stronger analysis correction, provided total column O_3 observations are available.

ACPD
15, 11573–11597, 2015

3.3 Analysis increment through the O_3 data assimilation

We assess the impact of the assimilated O_3 observations using analysis increments ($\boldsymbol{x}_a - \boldsymbol{x}_b$), which show the correction of the background state using the observations. It is calculated by the following variable transformation (Zhang et al., 2013; Zupanski, 2005)

$$\boldsymbol{x}_a - \boldsymbol{x}_b = \mathbf{P}_f^{1/2}\left\{\mathbf{I} + [\mathbf{Z}(\boldsymbol{x}_b)]^T\mathbf{Z}(\boldsymbol{x}_b)\right\}^{-1/2}\zeta \quad (6)$$

where ζ is the control variable in the ensemble space; the matrix in Eq. (6) is equal to the inverse of the square root Hessian of the cost function in Eq. (2); $\mathbf{Z}$ is the observation information matrix with column vectors $\mathbf{z}_i = \mathbf{R}^{-1/2}[h(\boldsymbol{x}_i) - h(\boldsymbol{x}_b)]$ (where the index i denotes the ensemble member).

Figure 4 shows the analysis increments ($\boldsymbol{x}_a - \boldsymbol{x}_b$) of chemical variables obtained by assimilating O_3 observations. By comparing Figs. 2 and 4 one can notice that the O_3 analysis increments are in agreement with background state uncertainties, as expected from Eq. (6). At 850 hPa, the O_3 analysis increment has an increase near the TC, but a decrease over China (Fig. 4a). At 200 hPa, however, there is an increase of O_3 near the TC, and marginal change over China (Fig. 4d). The strong positive response has the largest value of approximately 0.024 ppmv. At 200 hPa, positive O_3 analysis increments are correlated with positive NO_2 (Fig. 4e) and SO_2 (Fig. 4f) increments in the TC region, while the correlation is mixed for other regions. While NO_2 and SO_2 are not related to the TC at 850 hPa, the O_3 analysis increments are correlated with NO_2 (Fig. 4b) and SO_2 (Fig. 4c) increasing in central eastern China and Korea and decreasing in northeastern China.

Figure 5 shows the analysis increments ($\boldsymbol{x}_a - \boldsymbol{x}_b$) of atmospheric variables by O_3 assimilation. Corresponding to background state uncertainties, the analysis increments of wind show notable impact on both lower and upper pressure levels. Positive O_3 increments correspond to positive wind increments at 850 hPa (Fig. 5a), especially in the eye region, and to positive wind increments at 200 hPa (Fig. 5d) in the TC and

ACPD
15, 11573–11597, 2015

in the northeastern China and Korea. Regarding the temperature impact (Fig. 5b and e, respectively), the positive O_3 increments generate temperature cooling near the TC and warming over northeastern China. Regarding the water vapor mixing ratio, positive O_3 increments generate a reduction of water vapor mixing ratio (Fig. 5c and f, respectively) near the TC as well as in the eye region at both pressure levels. At 850 hPa, the water vapor mixing ratio is increasing with positive O_3 increments over the northeastern China (Fig. 5c). These results illustrate that chemical observations can impact not only the chemical variables but also the atmospheric variables, due to using the ensemble-based coupled atmosphere–chemistry background error covariance.

3.4 Validation of O_3 data assimilation

As a verification measure, we examine the O_3 assimilation impact on the cost function and on the root mean square (RMS) error with respect to O_3 observations, the same data used in the analysis. The cost function of O_3 driven by Eq. (2) has decreased from 0.36924×10^4 (background) to 0.30689×10^4 (analysis), i.e., it is reduced by approximately 16.9 %. The RMS error, calculated as

$$\mathrm{RMS_a} = \sqrt{\frac{1}{N}\sum[\boldsymbol{y} - h(\boldsymbol{x}_\mathrm{a})]^2} \quad \mathrm{RMS_b} = \sqrt{\frac{1}{N}\sum[\boldsymbol{y} - h(\boldsymbol{x}_\mathrm{b})]^2} \tag{7}$$

has also decreased from 0.16684×10^2 DU (background) to 0.15204×10^2 DU (analysis), i.e., by about 8.87 %. These results suggest that O_3 assimilation has produced a significant improvement in the initial conditions.

In addition, the impact of O_3 total column observations is also quantified in terms of the uncertainty reduction. With the Gaussian probability assumption, the information content of observations can be represented as the degrees of freedom for signal (d_s) (e.g., Rodgers, 2000) as

$$d_\mathrm{s} = \mathrm{tr}\left[\mathbf{I} - \mathbf{P}_\mathrm{a}\mathbf{P}_\mathrm{f}^{-1}\right] \tag{8}$$

ACPD
15, 11573–11597, 2015

where tr is trace functions, **I** is the identity matrix, and $\mathbf{P}_a$ and $\mathbf{P}_f$ are the analysis and background error covariances. Here d_s can also be expressed as

$$d_s = \sum_i \frac{\lambda_i^2}{1+\lambda_i^2} \tag{9}$$

where λ_i are the eigenvalues of the observation information matrix (e.g., Zupanski et al., 2007). Note from Eq. (9) that the d_s are strictly a non-negative measure: zero values indicate no impact of observations, while positive values indicate a reduction of uncertainty due to assimilation. As shown in Zupanski et al. (2007), the estimation of Eq. (9) is also useful in a reduced-rank setting of ensemble data assimilation.

In Fig. 6 we show the degree of freedom for signal of the assimilated total column O_3 observations. One can note that it generally coincides with the satellite path, and thus with observations, as expected. The area with the maximum impact is near the TC location, indicating that it is the area where the total column O_3 observation had the strongest impact. In agreement with the analysis increments, there exists a secondary maximum over northeast China, and a smaller one over the Yellow Sea. Given that the DA system includes atmospheric and chemical control variables, this result also indicates that O_3 total column observations have a positive impact on both the atmospheric and chemical components of the WRF-Chem system, especially in the TC area.

4 Conclusions

In this study, we investigated the impact of ozone (O_3) assimilation on the structure of a tropical cyclone (TC). We directly assimilated the total column O_3 from the Ozone Monitoring Instrument (OMI) in a coupled atmosphere–chemistry modelling system – the Weather Research and Forecasting (WRF) model coupled with Chemistry (WRF-Chem). An ensemble-based data assimilation, the maximum likelihood ensemble filter (MLEF) is employed and interfaced with the WRF-Chem. We include only a single data

ACPD
15, 11573–11597, 2015

assimilation cycle since the OMI observations are covering the model domain only once per day, and no other observations were available at the time. The use of a single data assimilation cycle limits the conclusions that can be drawn regarding the robustness of the data assimilation system, but it does not impact the performance and implications of using a coupled atmosphere–chemistry data assimilation system.

Our results show that the O_3 assimilation has a notable impact on the analyses of other chemical variables (e.g., NO_2 and SO_2) as well as O_3 itself, and atmospheric variables (e.g., wind, temperature and specific humidity), especially near the TC case considered. These atmospheric variables are closely related to the TC structure and other properties. The O_3 observations can affect other chemical and dynamical variables, and thus the TC itself. For example, temperature is related to development, wind to intensity, and specific humidity to precipitation of the TC. Therefore, the implied corrections of these variables in TC regions have a potential to improve the understanding, and eventually the forecast of TCs.

In our data assimilation experiments, the ensemble forecast error, given by the background error SD, appears reasonable with larger uncertainty over the TC area and also over eastern China. The RMS error reduction indicates an improvement of the optimal analysis state, while the degrees of freedom for signal indicate a reduction of the uncertainty of the optimal analysis.

As a future study, we plan to explore the longer data assimilation periods (e.g., several days) to assess the O_3 observation impact on the track, intensity and precipitation of TCs. Although we have only one available observation product per day for O_3, we anticipate a positive impact of assimilation. In addition to O_3, we plan to assimilate NO_2 and SO_2 observations, as well as atmospheric observations and all-sky infrared satellite radiances from a geostationary satellite that will be launched in the near future. Noting that NO_2 and SO_2 show high concentrations in East Asia, especially over eastern China, we expect to improve our understanding of the TC structure and the transboundary air pollution as well through assimilation of such chemical compositions from satellite observations.

ACPD
15, 11573–11597, 2015

Acknowledgements. This work is supported by the Korea Environmental Industry & Technology Institute through the Eco Innovation Program (ARQ201204015), and partly by the National Research Foundation of Korea grant (No. 2009-0083527) funded by the Korean government (MSIP). The third author would also like to acknowledge a partial support from the National Science Foundation Collaboration in Mathematical Geosciences Grant 0930265 and the NASA Modeling, Analysis and Prediction (MAP) Program Grant NNX13AO10G.

References

Apodaca, K., Zupanski, M., DeMaria, M., Knaff, J. A., and Grasso, L. D.: Development of a hybrid variational-ensemble data assimilation technique for observed lightning tested in a mesoscale model, Nonlin. Processes Geophys., 21, 1027–1041, doi:10.5194/npg-21-1027-2014, 2014.

Buehner, M.: Ensemble-derived stationary and flow-dependent background-error covariances, Q. J. Roy. Meteorol. Soc., 131, 1013–1043, 2005.

Carmichael, G. R., Sandu, A., Chai, T., Daescu, D. N., Constantinescu, E. M., and Tang, Y.: Predicting air quality: improvements through advanced methods to integrate models and measurements, J. Comput. Phys., 227, 3540–3571, 2008.

Carsey, T. P. and Willoughby, H. E.: Ozone measurements from eyewall transects of two Atlantic tropical cyclones, Mon. Weather Rev., 133, 166–174, 2005.

Chapman, E. G., Gustafson Jr., W. I., Easter, R. C., Barnard, J. C., Ghan, S. J., Pekour, M. S., and Fast, J. D.: Coupling aerosol-cloud-radiative processes in the WRF-Chem model: Investigating the radiative impact of elevated point sources, Atmos. Chem. Phys., 9, 945–964, doi:10.5194/acp-9-945-2009, 2009.

Elbern, H. and Schmidt, H.: A four-dimensional variational chemistry data assimilation scheme for Eulerian chemistry transport modeling, J. Geophys. Res., 104, 18583–18598, 1999.

Evensen, G.: The ensemble Kalman filter: theoretical formulation and practical implementation, Ocean Dynam., 53, 343–367, 2003.

Fletcher, S. J. and Zupanski, M.: A data assimilation method for log-normally distributed observational errors, Q. J. Roy. Meteorol. Soc., 132, 2505–2519, 2006.

ACPD
15, 11573–11597, 2015

Grell, G. A., Peckham, S. E., Schmitz, R., McKeen, S. A., Frost, G., Skamarock, W. C., and Eder, B.: Fully coupled "online" chemistry within the WRF model, Atmos. Environ., 39, 6957–6975, 2005.

Houtekamer, P. L. and Mitchell, H. L.: Data assimilation using an ensemble Kalman filter technique, Mon. Weather Rev., 126, 796–811, 1998.

Jang, K. I., Zou, X., De Pondeca, M. S. F. V., Shapiro, M., Davis, C., and Krueger, A.: Incorporating TOMS ozone measurements into the prediction of the Washington, DC, winter storm during 24–25 January 2000, J. Appl. Meteorol., 42, 797–812, 2003.

Kim, H. H., Park, S. K., Zupanski, D., and Zupanski, M.: 2010: Uncertainty analysis using the maximum likelihood ensemble filter and WRF and comparison with dropwindsonde observations in Typhoon Sinlaku (2008), Asia-Pac. J. Atmos. Sci., 46, 317–325, 2010.

Lahoz, W. A., Errera, Q., Swinbank, R., and Fonteyn, D.: Data assimilation of stratospheric constituents: a review, Atmos. Chem. Phys., 7, 5745–5773, doi:10.5194/acp-7-5745-2007, 2007.

Meena, G. S., Bhosale, C. S., and Jadhav, D. B.: Retrieval of stratospheric O_3 and NO_2 vertical profiles using zenith scattered light observations, J. Earth Syst. Sci., 115, 333–347, 2006.

Navon, I. M.: Data assimilation for numerical weather prediction: a review, in: Data Assimilation for Atmospheric, Oceanic and Hydrologic Applications, edited by: Park, S. K. and Xu, L., Springer, Berlin, Heidelberg, 21–65, 2009.

Ohara, T., Akimoto, H., Kurokawa, J., Horii, N., Yamaji, K., Yan, X., and Hayasaka, T.: An Asian emission inventory of anthropogenic emission sources for the period 1980–2020, Atmos. Chem. Phys., 7, 4419–4444, doi:10.5194/acp-7-4419-2007, 2007.

OMI Team: Ozone Monitoring Instrument (OMI) Data User's Guide, NASA, Greenbelt, 62, 2012.

Park, S. K. and Zupanski, D.: Four-dimensional variational data assimilation for mesoscale and storm-scale applications, Meteorol. Atmos. Phys., 82, 173–208, 2003.

Richter, A., Burrows, J. P., Nüß, H., Granier, C., and Niemeier, U.: Increase in tropospheric nitrogen dioxide over China observed from space, Nature, 437, 129–132, 2005.

Rodgers, C. D.: Inverse Methods for Atmospheric Sounding: theory and Practice, World Scientific, Singapore, 256 pp., 2000.

Rodgers, E. B., Stout, J., Steranka, J., and Chang, S.: Tropical cyclone-upper atmospheric interaction as inferred from satellite total ozone observations, J. Appl. Meteorol., 29, 934–954, 1990.

ACPD
15, 11573–11597, 2015

Silver, J. D., Brandt, J., Hvidberg, M., Frydendall, J., and Christensen, J. H.: Assimilation of OMI NO_2 retrievals into the limited-area chemistry-transport model DEHM (V2009.0) with a 3-D OI algorithm, Geosci. Model Dev., 6, 1–16, doi:10.5194/gmd-6-1-2013, 2013.

Skamarock, W. C., Klemp, J. B., Dudhia, J., Gill, D. O., Barker, D. M., Duda, M. G., Huang, X.-Y., Wang, W., and Powers, J. G.: A description of the Advanced Research WRF version 3. NCAR/TN-475+ STR, National Center For Atmospheric Research, Boulder, CO, 113 pp., 2008.

Stout, J. and Rodgers, E. B.: Nimbus-7 total ozone observations of western North Pacific tropical cyclones, J. Appl. Meteorol., 31, 758– 783, 1992.

Wang, K.-Y., Lary, D. J., Shallcross, D. E., Hall, S. M., and Pyle, J. A.: A review on the use of the adjoint method in four-dimensional atmospheric–chemistry data assimilation, Q. J. Roy. Meteor. Soc., 127, 2181–2204, 2001.

Wu, Y. and Zou, X.: Numerical test of a simple approach for using TOMS total ozone data in hurricane environment, Q. J. Roy. Meteor. Soc., 134, 1397–1408, 2008.

Yang, Q., W. I. Gustafson Jr., Fast, J. D., Wang, H., Easter, R. C., Morrison, H., Lee, Y.-N., Chapman, E. G., Spak, S. N., and Mena-Carrasco, M. A.: Assessing regional scale predictions of aerosols, marine stratocumulus, and their interactions during VOCALS-REx using WRF-Chem, Atmos. Chem. Phys., 11, 11951–11975, doi:10.5194/acp-11-11951-2011, 2011.

Zhang, R., Sanger, N. T., Orville, R. E., Tie, X., Randel, W., and Williams, E. R.: Enhanced NOx by lightning in the upper troposphere and lower stratosphere inferred from the UARS global NO2 measurements, Geophys. Res. Lett., 27, 685–688, 2000.

Zhang, S. Q., Zupanski, M., Hou, A. Y., Lin, X., and Cheung, S. H.: Assimilation of precipitation-affected radiances in a cloud-resolving WRF ensemble data assimilation system, Mon. Weather Rev., 141, 754–772, 2013.

Zou, X. and Y. Wu.: On the relationship between Total Ozone Mapping Spectrometer (TOMS) ozone and hurricanes, J. Geophys. Res.–Atmos., 110, D06109, doi:10.1029/2004JD005019, 2005.

Zupanski, M.: Maximum likelihood ensemble filter: theoretical aspects, Mon. Weather Rev., 133, 1710–1726, 2005.

Zupanski, M.: Theoretical and practical issues of ensemble data assimilation in weather and climate, in: Data Assimilation for Atmospheric, Oceanic and Hydrologic Applications, edited by: Park, S. K. and Xu, L., Springer, Berlin, Heidelberg, 67–84, 2009.

ACPD
15, 11573–11597, 2015

Zupanski, D., Hou, A. Y., Zhang, S. Q., Zupanski, M., Kummerow, C. D., and Cheung, S. H.: Applications of information theory in ensemble data assimilation, Q. J. Roy. Meteor. Soc., 133, 1533–1545, 2007.

Zupanski, M., Navon, I. M., and Zupanski, D.: The Maximum Likelihood Ensemble Filter as a non-differentiable minimization algorithm, Q. J. Roy. Meteor. Soc., 134, 1039–1050, 2008.

ACPD

15, 11573–11597, 2015

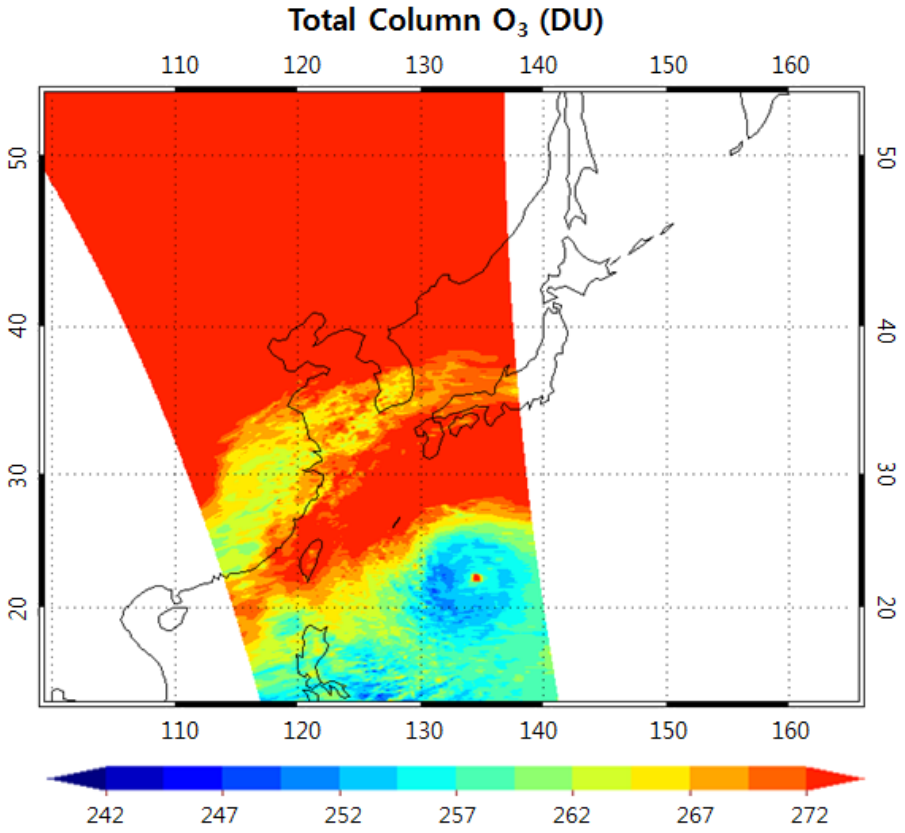

Figure 1. Total column O_3 (in DU) from OMI at 04:05 UTC, 3 September 2005.

ACPD
15, 11573–11597, 2015

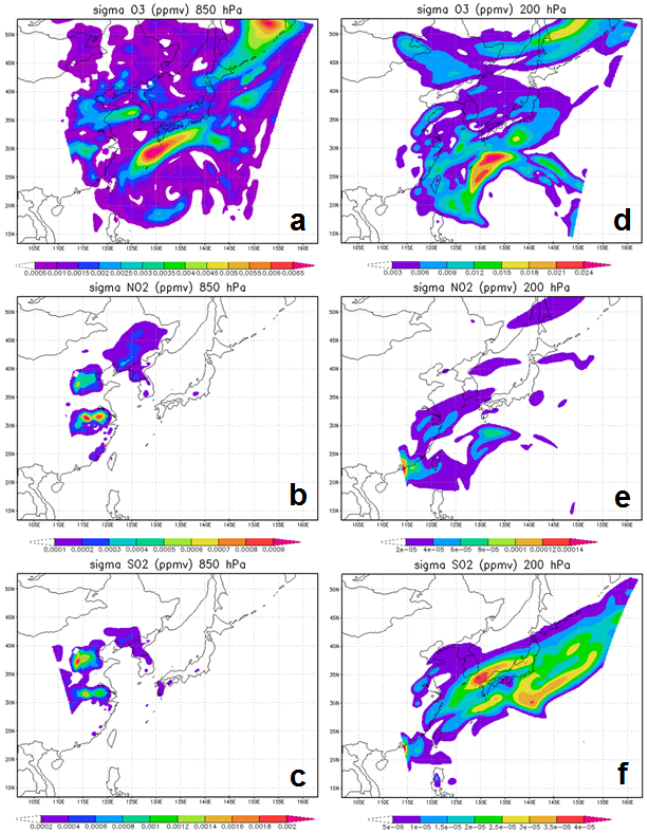

Figure 2. Standard deviation of background error covariance for chemical variables valid on 06:00 UTC, 3 September 2005 at 850 hPa (left panel) for **(a)** O_3, **(b)** NO_2 and **(c)** SO_2, and at 200 hPa (right panel) for **(d)** O_3, **(e)** NO_2 and **(f)** SO_2. Units are ppmv.

ACPD
15, 11573–11597, 2015

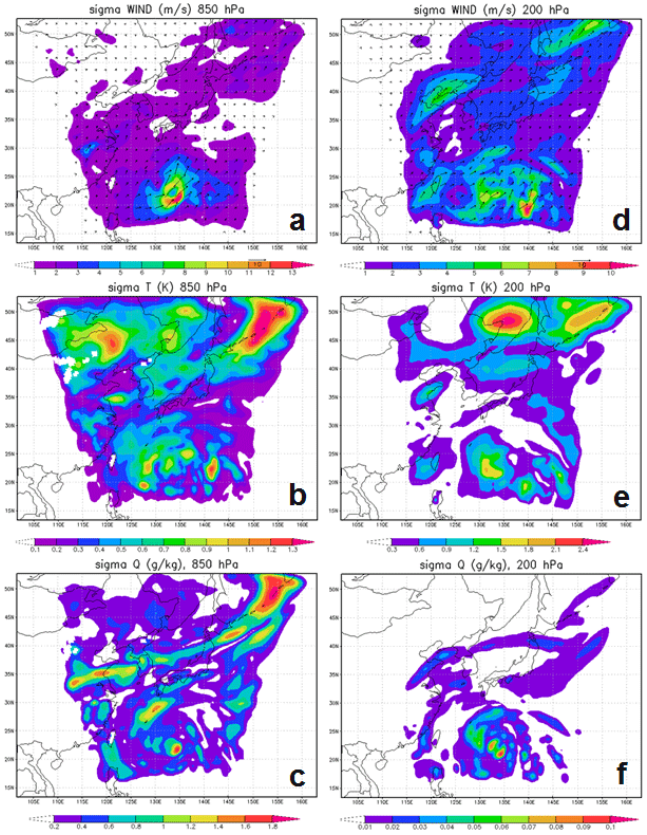

Figure 3. Standard deviation of background error covariance for atmospheric variables valid on 06:00 UTC, 3 September 2005 at 850 hPa (left panel) for **(a)** wind, **(b)** temperature and **(c)** water vapor mixing ratio, and at 200 hPa (right panel) for **(d)** wind, **(e)** temperature and **(f)** water vapor mixing ratio. Units are m s^{-1} for wind, K for temperature and g kg^{-1} for water vapor mixing ratio.

ACPD
15, 11573–11597, 2015

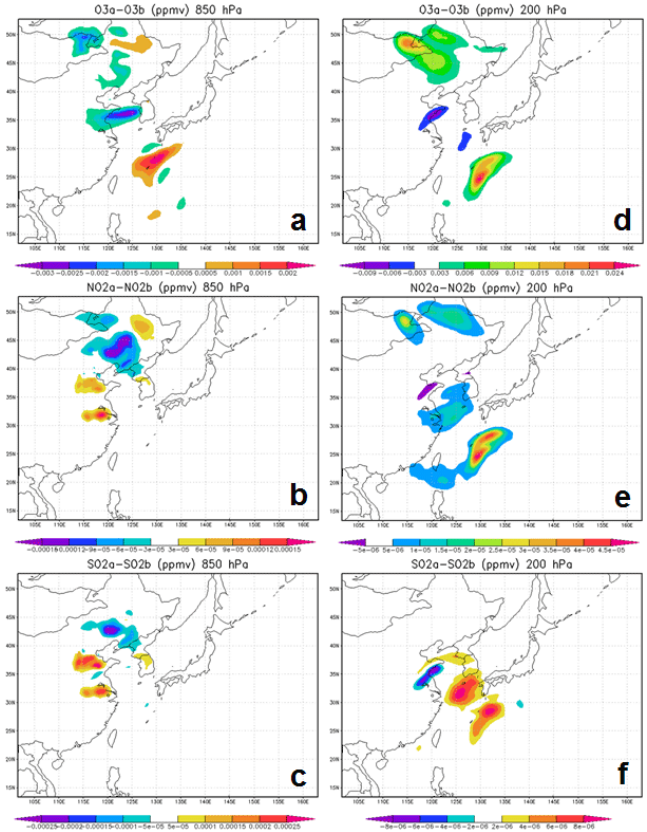

Figure 4. Same as in Fig. 2 except for analysis increment ($\boldsymbol{x}_a - \boldsymbol{x}_b$) of chemical variables in response to total column O_3. Units are ppmv.

ACPD
15, 11573–11597, 2015

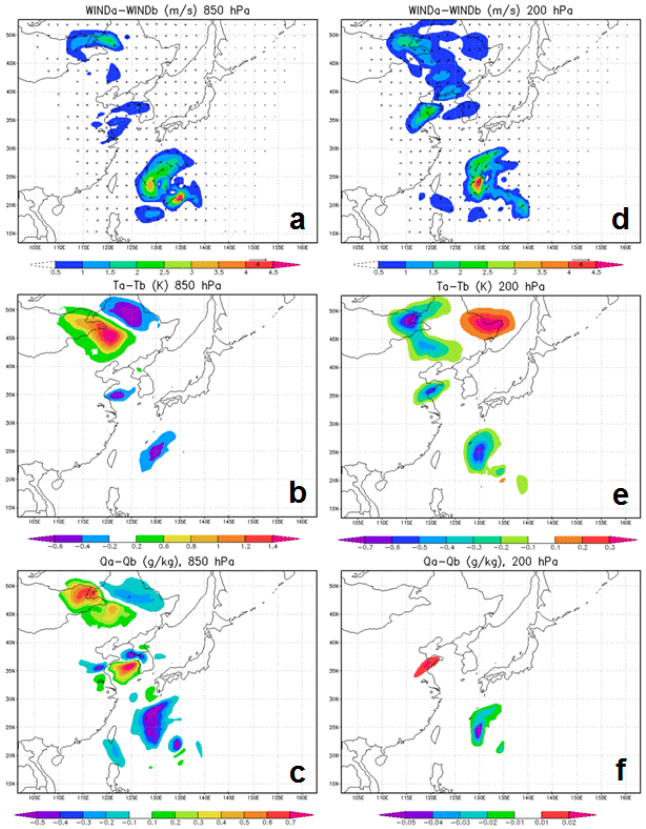

Figure 5. Same as in Fig. 3 except for analysis increment ($\boldsymbol{x}_a - \boldsymbol{x}_b$) of atmospheric variables in response to total column O_3. Units are m s^{-1} for wind, K for temperature and g kg^{-1} for water vapor mixing ratio.

ACPD
15, 11573–11597, 2015

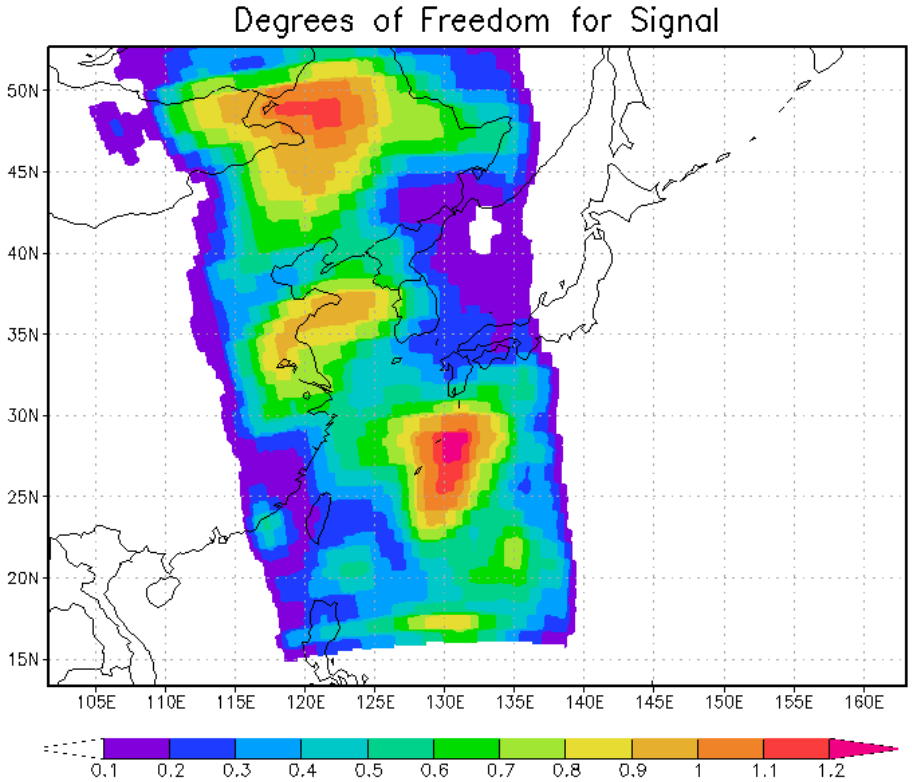

Figure 6. Degrees of Freedom for signal of assimilated total column O_3 observation valid at 06:00 UTC, 3 September 2005. The units are non-dimensional.

ACPD
15, 11573–11597, 2015